

Detection of the gravitational memory effect in LISA using triggers from ground-based detectors

Sourath Ghosh¹, Alexander Weaver¹, Jose Sanjuan,² Paul Fulda¹ and Guido Mueller^{1,3}

¹Physics Department, University of Florida, Gainesville 32611, USA

²Department of Aerospace Engineering, Texas A&M University, College Station 77843, USA

³Max Planck Institute for Gravitational Physics (Albert-Einstein-Institut), Hannover D-30167, Germany

 (Received 9 February 2023; accepted 31 March 2023; published 28 April 2023)

The LIGO-Virgo-KAGRA (LVK) Collaboration has detected gravitational waves (GWs) from 90 compact binary coalescences. In addition to fortifying the linearized theory of general relativity (GR), the statistical ensemble of detections also provides prospects of detecting nonlinear effects predicted by GR, one such prediction being the nonlinear gravitational memory effect. For detected stellar and intermediate mass compact binaries, the induced strain from the memory effect is 1 or 2 orders below the detector noise background. Additionally, since most of the energy is radiated at merger the strain induced by the memory effect resembles a step function at the merger time. These facts motivate the idea of coherently stacking up data streams from recorded GW events at these merger times so that the cumulative memory strain is detected with a sufficient signal to noise ratio (SNR). GW detectors essentially record the integrated strain response at timescales of the round-trip light travel time, making future space-based long arm interferometers like the Laser Interferometer Space Antenna (LISA) ideal for detecting the memory effect at low frequencies. In this paper, we propose a method that uses the event catalog of ground-based detectors and searches for corresponding memory strains in the LISA data stream. Given LVK's O3 science run catalog, we use scaling arguments and assumptions on the source population models to estimate the run-time required for LISA to accumulate a memory SNR of 5, using triggers from current and future ground-based detectors. Finally, we extend these calculations for using beyond LISA missions like Advanced Laser Interferometer Antenna (ALIA), Advanced Millihertz Gravitational-wave Observatory (AMIGO), and Folkner to detect the gravitational memory effect. The results for LISA in conjunction with Einstein Telescope or a combination of Einstein Telescope and Cosmic Explorer indicate a possible detection of the memory effect within the 10 year LISA mission lifetime. The corresponding results for beyond LISA missions are even more promising.

DOI: [10.1103/PhysRevD.107.084051](https://doi.org/10.1103/PhysRevD.107.084051)

I. INTRODUCTION

The first direct detection of gravitational wave (GW) radiation from compact binary sources was made by the LIGO Scientific Collaboration in 2015. This detection and the 89 since validate Einstein's general relativity (GR) in the linearized approximation. The next step in the puzzle is to use the ensemble of detected events to extract salient features predicted by full nonlinear GR. In 1991, Christodoulou [1] estimated the strain induced by one particular ramification of nonlinear GR, the gravitational memory effect, which predicts a permanent nonzero strain in space-time after the passage of the GW wave. This

phenomenon for compact binary sources was estimated to be only 1 or 2 orders of magnitude below the GW strain predicted by linearized GR. Shortly after Christodoulou's findings, Wiseman, Will, and Thorne [2] identified that Christodoulou's memory effect is essentially sourced by the outgoing radiation itself, i.e., in particle energy language, the additional strain induced by the energy of moving gravitons. Consequently, they derive an expression for the time-dependent strain induced by the memory effect in the transverse traceless (TT) gauge, which matches Christodoulou's findings in the $t \rightarrow \infty$ asymptotic limit:

$$h_{\text{Mem}ij}(t) = \frac{4G}{rc^4} \int_{-\infty}^t \int_{\Omega'} \frac{dE}{dt d\Omega'} \frac{n'_i n'_j}{1 - \vec{n}' \cdot \vec{z}'} d\Omega' dt. \quad (1)$$

Here $\frac{dE}{dt d\Omega'}$ is the energy flux of the radiated gravitational wave per unit solid angle. The primed coordinates represent

Published by the American Physical Society under the terms of the [Creative Commons Attribution 4.0 International license](https://creativecommons.org/licenses/by/4.0/). Further distribution of this work must maintain attribution to the author(s) and the published article's title, journal citation, and DOI.

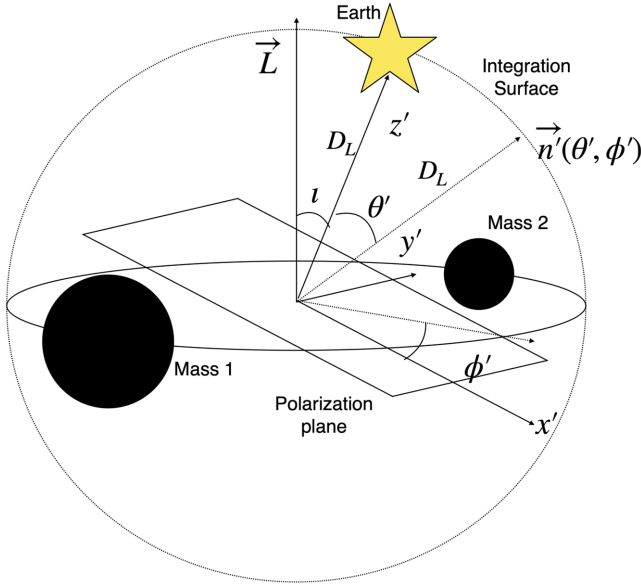


FIG. 1. Source frame coordinate system for compact binary sources. z' axis is fixed as the line of sight direction, and ι is the inclination angle, i.e., the angle between the source angular momentum \vec{L} and the line of sight. Furthermore x' axis is defined to be coplanar to z' and \vec{L} , while y' axis is defined so that x', y', z' form an orthogonal right-handed coordinate system.

the coordinates of the source frame (see Fig. 1), \vec{z}' being the line of sight vector. Spatial integration is over the entire spherical wave front centered on the source passing by the detector at time t . The time integration represents the addition of these infinitesimal strain contributions from these wave fronts over the entire past right up to the present, thus representing the “memory.” Figure 2 shows the strain and the

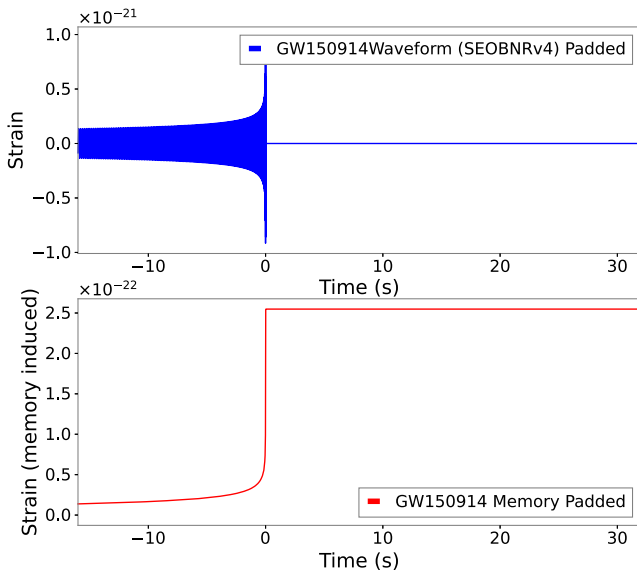


FIG. 2. Top panel: GW150914 strain waveform (SEOBNRv4 approximant). Bottom panel: the induced memory strain sourced by the gravitational wave radiation.

corresponding induced memory strain for GW150914, the first event detected by LIGO detectors [3], assuming it to be an equal mass binary and using a simplified version of Eq. (1); see Sec. II.

We see that, for stellar and intermediate mass compact binaries, the memory waveform is an order of magnitude weaker than the radiation waveform. This necessitates using an ensemble stack of detected events wherein the cumulative signal to noise ratio (SNR) statistic on an average scales with the square root of the number of detections [4]. In recent works, Grant and Nichols [5] have estimated the required detector run-time to detect gravitational memory directly in the data streams of ground-based detectors and Gasparotto *et al.* [6] have done an analogous calculation for detecting gravitational memory of Laser Interferometer Space Antenna (LISA) binaries directly in the LISA [7] data stream.

In this work, we propose an alternative idea of searching for memory imprints in data streams of future space-based GW detectors (LISA [7] and follow-on LISA-like mission concepts Advanced Laser Interferometer Antenna (ALIA) [8], Advanced Millihertz Gravitational-wave Observatory (AMIGO) [9] and Folkner [10]) using event triggers from ground-based detectors [LIGO, Einstein Telescope (ET) [11], and Cosmic Explorer (CE) [12,13]]. LISA is scheduled to be launched in the late 2030s and will be the first GW detector sensitive to sources radiating at millihertz frequencies (the frequency band being 0.1 mHz–1 Hz). The proposed interferometer design entails three spacecraft (denoted by SC_1 , SC_2 and SC_3 in this paper) oriented in an approximate 2.5 Gm equilateral triangle, each one hosting a pair of free falling test masses (TMs). The combination of six inter-TM distance measurements (aboard different spacecraft) is the probe for gravitational wave strain measurement. The follow-on space missions scheduled for launch in the second half of the century adopt a similar interferometric layout with different arm lengths and noise budgets (see Sec. V), thus making them sensitive to different frequency bands in the subhertz regime.

One of the advantages of using data streams of space-based GW detectors is the fact that the round-trip light travel time is 1–4 orders of magnitude greater than the rise time of the memory waveform. Divakarla in his thesis [14] showed that the rise time scales as $\mathcal{O}(\frac{GM_{\text{total}}}{c^3})$ and we calculate the rise time (using the same definition) for the most massive equal mass binary considered in this paper ($M_{\text{total}} = 10^4 M_{\odot}$) to be about 0.5 s, which is a factor of 33 less than the round-trip light travel time of LISA [7]. This difference in timescales results in the memory signal’s duration being predominantly determined by the round-trip light travel time, the morphology of the signal being determined predominantly determined by the source’s sky position (with respect to the detector), and all the other parameters determining only the amplitude of the signal (see Fig. 4). This enables us to use a simple stacking

algorithm in the time domain, analogous to the one used in Lasky *et al.* [4], with the benefit of being able to use a single template to compute the memory SNR of all events. We would like to caution the reader here that the data stacking algorithm used in this paper hinges on the assumption that the sign of the memory signal is known perfectly. As it stands, the detection of the dominant $l = 2, m = \pm 2$ oscillatory mode gives a fairly accurate estimate of the memory signal magnitude but is insufficient to determine the sign. Lasky *et al.* [4] discuss this in detail and provide a solution which relies on the detectability of higher-order modes.

The paper is organized as follows: Section II expands on Eq. (1) and calculates the memory waveform response in LISA's TDI X data stream. In Sec. III we introduce a cumulative SNR statistic formed via the aforementioned stacking or combination of individual memory effects, utilizing GW150914's memory effect as a toy model for estimating the effects of stacked signal on this cumulative SNR. We also use the existing catalog of LIGO events to estimate the LISA detector run-time required to accumulate enough memory SNR to cross the preset threshold of 5. Section IV scales this calculation to estimate the run-time required if using predicted catalogs from future ground-based detectors triggers like LIGO (with $A^\#$ sensitivity), Cosmic Explorer and Einstein Telescope instead of LIGO triggers. Section V extends the calculation in Sec. IV to future LISA-like mission concepts, namely ALIA, AMIGO, and Folkner. Section VI discusses conclusions and future implications.

II. LISA DETECTOR RESPONSE TO MEMORY WAVEFORM

The choice of source frame coordinates in Fig. 1 ensures that the memory strain waveform is polarized in the $x' - y'$ (+) direction. Furthermore, the memory strain tensor of Eq. (1) can be simplified to an expression involving luminosity distance D_L , the inclination angle ι and the largely dominant $l = 2, m = 2$ spin-weighted spherical harmonic for equal mass nonspinning binary systems [14] (note: all calculations in this paper assume equal mass binaries with zero spin)

$$h(t) = h_{\text{Mem}+}(t) = h_{\text{Mem}11} = -h_{\text{Mem}22} = \frac{D_L}{192\pi c} \sin^2 \iota (17 + \cos^2 \iota) \int_{-\infty}^t |\dot{h}_{22}(t)|^2 dt, \quad (2)$$

$$h_{\text{Mem}\times}(t) = h_{\text{Mem}12} = h_{\text{Mem}21} = 0. \quad (3)$$

To calculate the memory-induced strain response in LISA arms, we follow Ref. [15] and introduce a new set of "detector frame" coordinates defined in Fig. 3.

With these conventions, the strain responses $[z_{12}(t), z_{13}(t)]$ of the two LISA arms associated with SC_1 (assuming the arm lengths to be equal and constant over light travel timescales) is given in terms of the memory strain $h(t)$, the inter-SC light travel time $\tau = 8.3$ s, the polarization angles Ψ_{12} and Ψ_{13} and the angles the arms subtend along the propagation direction θ_{12}, θ_{13} [15]:

$$z_{1j}(t) = \frac{\cos(2\Psi_{1j})}{2\tau} \left(\int_{t-2\tau}^t h(t) dt - \cos\theta_{1j} \left(\int_{t-\tau(1+\cos\theta_{1j})}^t h(t) dt - \int_{t-2\tau}^{t-\tau(1+\cos\theta_{1j})} h(t) dt \right) \right); \quad j = 2, 3. \quad (4)$$

The first integral represents the arm response for waves incoming orthogonal to the detector plane while the second and third integrals represent the corrections for oblique incidence resulting in the wave arriving at slightly different times at every spacecraft.

LISA's postprocessing algorithm, time delay interferometry (TDI) [16] is designed to mitigate the dominant laser frequency noise to the subpicometer level, after which shot noise is expected to dominate above 3 mHz and acceleration noise dominates below 3 mHz. We assume a shot-noise-dominated noise background with a white noise displacement amplitude spectral density at each science photodiode given by [17]

$$\tilde{n}_s = \frac{5 \text{ pm}}{\sqrt{\text{Hz}}}. \quad (5)$$

Thus the noise contribution to the single arm responses measured on SC_1 are given by

$$n_{1j}(t) = n_{s1j}(t) - n_{s,j1}(t - 2\tau); \quad j = 2, 3, \quad (6)$$

where τ is the one-way light travel time and n_{sij} is the shot noise measured on the science photodiode on spacecraft i which is linked to spacecraft j . The total single arm and the interferometer strain responses are given by

$$s_{1j}(t) = z_{1j}(t) + n_{1j}(t); \quad j = 2, 3, \quad (7)$$

$$\Delta_1(t) = s_{12}(t) - s_{13}(t). \quad (8)$$

For this paper, we use the TDI_{1,0} X data stream, which results from the first-generation TDI algorithm that

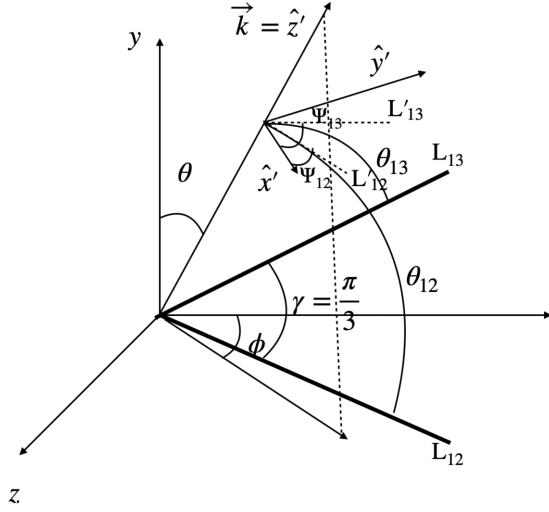


FIG. 3. Detector frame coordinate system. x', y', z' represent the source frame coordinates. L_{12}, L_{13} represent the LISA arms with SC_1 being the primary spacecraft and SC_2, SC_3 being the far spacecraft. The detector x axis is fixed at the small angle bisector of the arms while the z axis is fixed to be perpendicular to both arms. The polarization angles Ψ_{12} and Ψ_{13} are then defined as the angles made by the LISA arms projected onto the polarization plane (L'_{12}, L'_{13}) with the x' axis.

assumes a constant arm length over the timescale of the round-trip light travel time. Additionally for computational simplicity, we also assume equal interferometer arms. With this assumption the $TDI_{1,0} X$ [16] response is simplified to

$$X_{1,0}(t) = \Delta_1(t) - \Delta_1(t - 2\tau). \quad (9)$$

Note that, for LISA's science operations, it is pertinent to account for unequal arms to subtract out laser frequency noise. Given that LISA's arm length mismatch corresponds to a light travel time $\Delta\tau < 130$ ms we estimate the resulting correction to the memory SNR computed with the equal arm assumption to be smaller by a factor of $O(10^{-3})$. Furthermore, LISA's science operation will most likely employ the second-generation TDI algorithm TDI 2.0 which accounts for changes in arm length during one round-trip light travel time. While we do not expect significant (if any) changes in the memory SNR computed with the $TDI_{1,0} X$ data stream, we aim to use TDI 2.0 data streams in future works.

Figure 4 illustrates the length change induced by the GW150914 memory in the LISA interferometer and $TDI_{1,0} X$ responses, for a fixed azimuthal angle ϕ with different polar angles (θ in Fig. 3) and corresponding optimal values [with respect to the interferometer (IFO) and TDI responses] of the polarization angles Ψ_{12} and Ψ_{13} . Note that the choice of polarization angles chosen for the figure is optimal for the positively signed memory effect. The transformation $(\Psi_{12}, \Psi_{13}) \rightarrow (\frac{\pi}{2} + \Psi_{12}, \frac{\pi}{2} + \Psi_{13})$ gives the corresponding negatively signed memory effect.

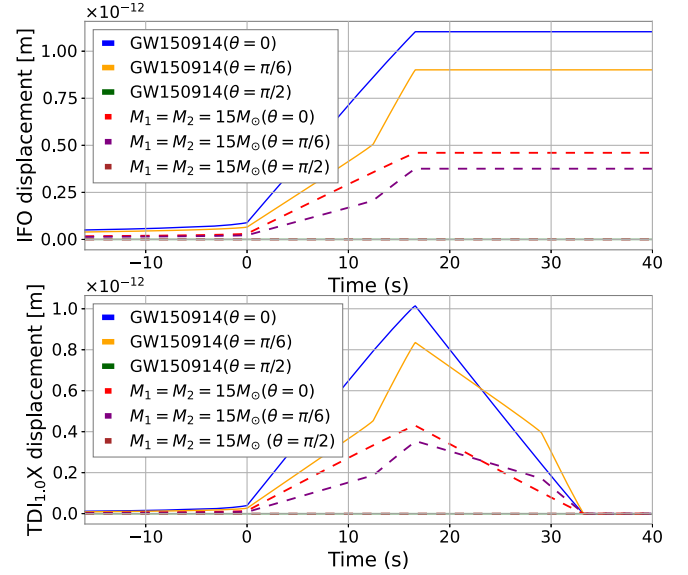


FIG. 4. Plots for the GW150914 memory induced test mass (TM) displacement in the LISA IFO (top panel) and $TDI_{1,0} X$ (bottom panel) data streams. Traces are produced with the azimuthal angle fixed at $\phi = 0$ and values for polarization angles Ψ_{12} and Ψ_{13} that give optimal positively signed memory effect. For comparison, similar traces are plotted for a $15M_{\odot}$ equal mass zero spin compact binary situated at the same luminosity distance.

III. MEMORY SNR CALCULATION

As evident from Fig. 5, shot noise dominates the GW150914 response and the same is true for other stellar and intermediate mass compact binaries. Furthermore, from Eq. (4) and Fig. 4, it is evident that the memory response in TDI X resembles (further quantified in Sec. III B) a triangular pulse $[h_{\Delta}(t)]$ with a base of 4τ starting from the coalescence time. These two observations motivate the idea of looking up the coalescence times of recorded GW events and creating a composite data stream, $X_{\text{stack}}(t)$, by stacking up the TDI data snippets (X_i) of length 4τ s that start at these

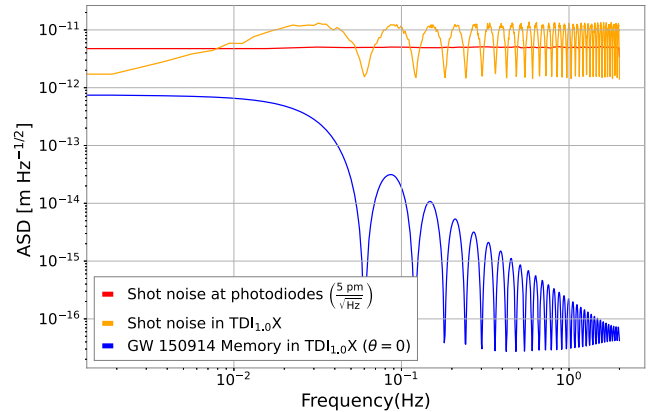


FIG. 5. GW150914 memory (optimal orientation) against shot noise background in $TDI_{1,0} X$.

coalescence times. This stacking is performed with the appropriate weight factors (w_i) and is processed through a common-matched filter with a triangular pulse template. [Note: Excluding the effects of suboptimal inclination angle and sky direction angles (see Sec. III B), the use of a triangular pulse template as opposed to the template derived from the memory waveform itself results in a $< 0.2\%$ loss in SNR in the worst-case scenario, the worst-case scenario being a binary with $M_{\text{Tot}} = 10^4 M_\odot$].

We divide this section into three subsections. In Sec. III A, we define the cumulative SNR statistic and define the corresponding detection threshold SNR value used for the extraction of memory signals. Following this in Sec. III B, we apply our SNR statistic on a stack of GW150914-like events. Accounting for expected loss of SNR due to suboptimal detector orientation (orange and green traces in Fig. 4) and losses in the source power due to source inclination angle [Eq. (2)], we calculate an estimate of the number of GW150914-like events required to cross the SNR threshold. Finally in Sec. III C, we use scaling arguments to calculate the expected memory SNR in LISA accumulated with events detected during LIGO's O3 science run [18,19]. We estimate the expected time required for LIGO-like detectors (with O3 sensitivity) to provide enough detections for the cumulative memory SNR in LISA to cross the preset threshold.

A. The memory SNR statistic

In this paper, the definition of SNR of a generic data stream $d(t)$ matched to a triangular pulse template of unit height $h_\Delta(t)$ is given by

$$\text{SNR} = \frac{\vec{d}(t)^\dagger C^{-1} \vec{h}_\Delta(t)}{\sqrt{\vec{h}_\Delta(t)^\dagger C^{-1} \vec{h}_\Delta(t)}}, \quad (10)$$

where \dagger represents the transpose operation and C is the noise covariance matrix of $d(t)$ whose elements are given by

$$C_{kl} = \langle (\text{noise}(d[k])^*) (\text{noise}(d[l])) \rangle, \quad (11)$$

where $d[k]$ and $d[l]$ represent the k th and l th elements, respectively, of the data stream $d(t)$ and the angled brackets represent an ensemble average. This definition of SNR is equivalent to the well-known frequency domain definition of the optimum matched filter SNR used in LIGO's modeled search analysis [20]. For a zero-mean noise background, we see that, in the absence of a signal, the SNR statistic in Eq. (10) has zero mean and standard deviation (σ_{SNR}) of unity. This motivates us to use an SNR threshold of 5 to claim a 5σ detection.

As mentioned above, the data stream for our calculation is a weighted combination of N TDI data snippets with a background dominated by shot noise. Therefore, the data stream is given by

$$\vec{d}(t) = \sum_{i=1}^N w_i \vec{X}_i(t) \quad (12)$$

and the covariance matrix takes the form

$$C = \left(\sum_{i=1}^N w_i^2 \right) \langle n_{\text{shot}}^2(t) \rangle \begin{pmatrix} 8\mathbf{I}_{2\tau \times 2\tau} & -4\mathbf{I}_{2\tau \times 2\tau} \\ -4\mathbf{I}_{2\tau \times 2\tau} & 8\mathbf{I}_{2\tau \times 2\tau} \end{pmatrix} \quad (13)$$

$$= \left(\sum_{i=1}^N w_i^2 \right) C_{1 \text{ event}}. \quad (14)$$

Here $\langle n_{\text{shot}}^2(t) \rangle = \tilde{n}_s^2 \frac{f_{\text{LISA}}}{2}$ is the variance of the shot noise in each science photodetector [derived from Eq. (5)], LISA's sample rate being $f_{\text{LISA}} = 4$ Hz and the highest frequency in band being given by the Nyquist criterion to be 2 Hz. Additionally, $\mathbf{I}_{2\tau \times 2\tau}$ represents a 66×66 identity matrix [$66 = \text{greatest integer}(2\tau f_{\text{LISA}})$]. Furthermore, $C_{1 \text{ event}}$ represents the covariance matrix of an individual TDI data stream.

The optimum choice of weights w_i corresponds to the choice that maximizes the expected value of the SNR statistic in the presence of a signal. Modeling the signal component of X_i to be a triangle of known height (and known sign) a_i , we have

$$\text{signal}(\vec{X}_i(t)) \approx a_i \vec{h}_\Delta(t). \quad (15)$$

Therefore, using Eq. (10), the expected value of SNR in the presence of a signal is given by

$$\langle \text{SNR} \rangle = \left(\frac{\sum_{i=1}^N a_i w_i}{\sqrt{\sum_{j=1}^N w_j^2}} \right) \sqrt{\vec{h}_\Delta(t)^\dagger C_{1 \text{ event}}^{-1} \vec{h}_\Delta(t)}, \quad (16)$$

which has a maximum value of

$$\langle \text{SNR} \rangle_{\text{Max}} = \sqrt{\left(\sum_{i=1}^N a_i^2 \right)} \sqrt{\vec{h}_\Delta(t)^\dagger C_{1 \text{ event}}^{-1} \vec{h}_\Delta(t)} \quad (17)$$

for the choice of weights $w_i = a_i$.

B. Memory SNR of GW150914-like events in LISA

Using the definition of SNR in Sec. III A we calculate the memory SNR accumulated by stacking GW150914-like events. We simulate multiple TDI X data streams each composed of the GW150914 memory signal with optimal source inclination angle ($\iota = \pi/2$) and optimal detector orientation ($\theta = 0$ in Fig. 3) in a randomly generated shot noise background. Figure 6 shows the accumulation of SNR as a function of number of stacked event data streams. We see that the signal rises above the noise background on stacking about five data streams and eventually end up with

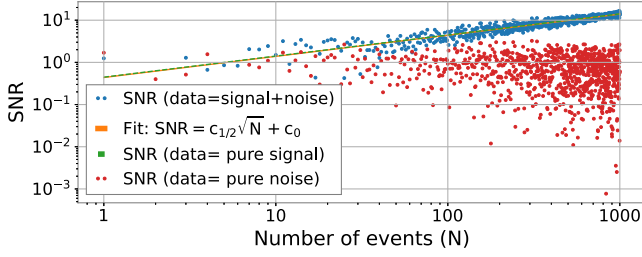


FIG. 6. Scaling of matched filter SNR with number of optimally oriented GW150914 events.

an SNR of 14.11 on stacking 1000 data streams. The figure also confirms the square-root dependence of the SNR on the number of events. From this, we can extrapolate and estimate the average SNR of one optimally oriented GW150914 event to be 0.45 and therefore require a stack of about 125 optimally oriented GW150914-like events to cross the SNR threshold of 5.

We now use Eqs. (2) and (4) to estimate the effects of averaging over inclination angle ι and the sky-direction angles (θ, ϕ) , i.e., to estimate the SNR lost from the diminished signal strength of suboptimally oriented events and the SNR lost from using the triangular template for extracting these suboptimally oriented events. These three angles are assumed to be mutually independent and uniformly distributed. We use Eq. (2) to estimate the effects of averaging over inclination angle ι and Eq. (4) to estimate the effects of averaging over the sky-direction (θ, ϕ) and polarization (Ψ_{12}, Ψ_{13}) angles. The four angles ι , θ , ϕ and $\Psi_+ = \Psi_{12} + \Psi_{13}$ are mutually independent and are assumed to be uniformly distributed, while $\Psi_- = \Psi_{12} - \Psi_{13}$ is a function of θ and ϕ .

The ratio of the SNR averaged by the inclination angle and the maximum SNR is given by

$$\frac{\langle \text{SNR}(\iota) \rangle_{\iota}}{\text{SNR}(\iota = \pi/2)} = \frac{\langle \sin^2 \iota (17 + \cos^2 \iota) \rangle}{17} \approx 0.50. \quad (18)$$

Similarly, we use Eq. (4) to estimate the fractional drop in SNR as we move away from orthogonal incidence to the plane of the detector (see Fig. 7). Consequently, average over sky-direction and polarization angles as a fraction of the maximum SNR ($\theta = 0, \Psi_+ = \pi/2$)

$$\frac{\langle \text{SNR} \rangle_{\theta, \phi, \Psi_+}}{\text{SNR}(\theta = 0, \Psi_+ = \pi/2)} = 0.55 \frac{2}{\pi}. \quad (19)$$

From Eqs. (18) and (19), we deduce the averaged memory SNR from one GW150914-like event to be $0.08 (= [(0.5)(0.55 \frac{2}{\pi})](0.45))$. Thus, approximately 4000 randomly oriented GW150914-like events are needed to cross an SNR threshold of 5.

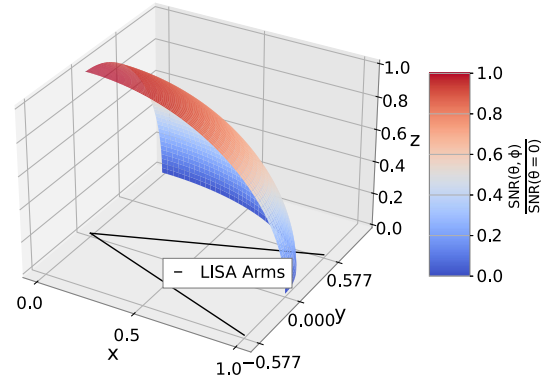


FIG. 7. Variation of SNR with sky direction with optimal polarization angles ($\Psi_+ = \pi/2$).

C. Memory SNR of the LIGO O3 catalog

To get a rough estimate of the memory SNR from the LIGO O3 catalog events, we estimate the scaling relation between the memory amplitude (a) and the binary chirp mass (\mathcal{M}_c) for the SEOBNRv4 waveform model class in Fig. 8.

From the graph, we infer an empirical scaling relation:

$$a \propto D_L^{-1} (\mathcal{M}_c)^\alpha; \quad \alpha = 0.96. \quad (20)$$

[Note that the D_L^{-1} dependence comes from Eq. (2).] Furthermore, for the events in the LIGO catalog with O3 sensitivity [18,19], we see that

$$\sqrt{\sum_{\text{Catalog Events}} D_L^{-2} (\mathcal{M}_c)^{2\alpha}} \gtrsim 1.9 (D_L^{-1} (\mathcal{M}_c)^\alpha)_{150914} \quad (21)$$

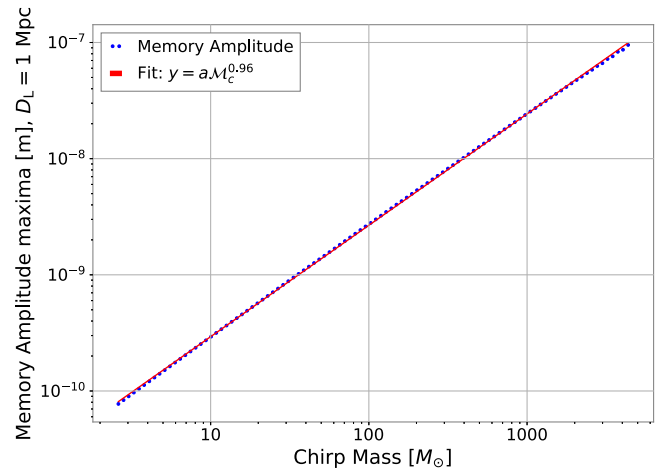


FIG. 8. Memory waveform maxima scaling with chirp mass \mathcal{M}_c for binaries located at a luminosity distance $D_L = 1$ Mpc.

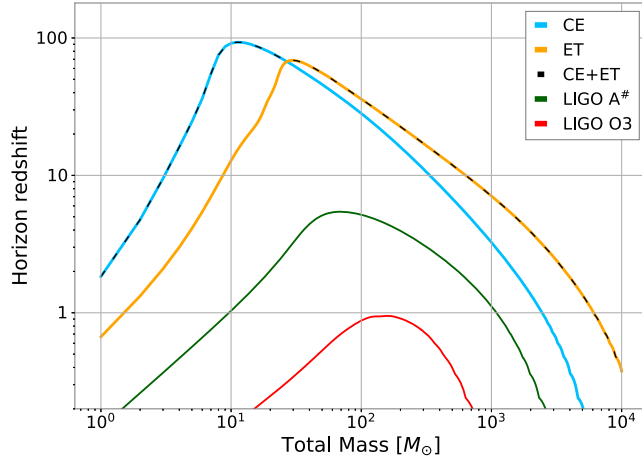


FIG. 9. Horizon redshifts of ground-based detectors [22]. The traces represent the maximum redshift at which optimally oriented equal mass binaries can be detected with an SNR threshold of 8.

$$\therefore \sqrt{\sum_{\text{Catalog Events}} a^2} \gtrsim 1.9a_{150914} \quad (22)$$

and, consequently, from Eq. (17) the cumulative memory SNR of the O3 catalog is related to the memory SNR of GW150914 by

$$\text{SNR}_{\text{O3 Catalog}} \gtrsim 1.9, \quad \text{SNR}_{150914} = 0.1045, \quad (23)$$

which means that the LIGO O3 run will have to be repeated at most 2100 times over to cross the SNR threshold of 5.

From Refs. [18,19,21], we find the run-time for LIGO's O3 run to be $t_{\text{LIGO-O3}} \approx 0.95$ yr. Thus for LIGO detectors with O3 sensitivity, the cumulative memory SNR in LISA would cross the detection threshold in ≈ 2000 yr of concurrent operation.

That being said, we do expect to have far more sensitive ground-based detectors like LIGO with A# sensitivity, Cosmic Explorer, and Einstein Telescope to be up and running when LISA starts its science operation. From the horizon redshift curves plotted in Fig. 9, we expect the event detection rate from these detectors to be much higher than LIGO with O3 sensitivity, thus resulting in a much faster memory SNR accumulation in LISA. Section IV provides estimates for the required run-time to detect gravitational memory in LISA from the projected catalogs of these future ground-based detectors.

Note on the error analysis: In this section, we calculated the expected number of GW150914-like events, the expected number of LIGO O3 catalogs, and consequently, the expected time required for LISA (using the LIGO O3 catalog) to accumulate a memory SNR of 5. Assuming perfect knowledge of the waveform parameters, the

TABLE I. Time taken to accumulate an SNR threshold of 5 in LISA's TDI data stream using triggers from projected CE, ET and LIGO A# catalogs.

Detector(d)	$\frac{\text{SNR}^d}{\text{SNR}^{\text{LIGO O3}}}$	Time for memory detection with LISA [yr]
CE	8.69	26
ET	18.94	6
LIGO A#	4.13	120
LIGO O3	1	2000
CE + ET	18.94	6

TABLE II. Time taken to accumulate a SNR threshold of 5 in TDI data streams of LISA, ALIA, AMIGO and Folkner using triggers from projected CE, ET and LIGO A# catalogs.

Detector(d)	$\frac{\text{SNR}^d}{\text{SNR}^{\text{LIGO O3}}}$	Time for memory detection [yr]			
		LISA	AMIGO	ALIA	Folkner
CE	8.69	26	2.3×10^{-1}	9×10^{-2}	1.4×10^{-1}
ET	18.94	6	4.8×10^{-2}	1.9×10^{-2}	3.1×10^{-2}
LIGO A#	4.13	120	1.0	0.4	0.7
LIGO O3	1	2000	17	7	11
CE + ET	18.94	6	4.8×10^{-2}	1.9×10^{-2}	3.1×10^{-2}

uncertainty in the values quoted for these three quantities is solely attributed to the uncertainty in the SNR statistic [Eq. (10)]. The SNR statistic has unit variance, and, thus, the upper and lower bounds of the 1σ error bar for the aforementioned quantities correspond to values that are expected to give an SNR of 5.5 and 4.5, respectively. Additionally, the SNR is proportional to the square root of these quantities which results in the upper and lower 1σ error bounds for these quantities being 21% ($= \frac{5.5^2 - 5^2}{5^2} \times 100\%$) above and 19% ($= \frac{5^2 - 4.5^2}{5^2} \times 100\%$) below the quoted mean value, respectively. Assuming perfect knowledge of the astrophysical event rates and source distributions, the same error bar applies for values of required detector run-time quoted in Tables I and II.

IV. ESTIMATING MEMORY SNR IN LISA USING TRIGGERS FROM FUTURE GROUND-BASED DETECTORS

In this section we estimate the expected rate of accumulation of memory SNR corresponding to triggers from future ground-based GW detectors, namely, Advanced LIGO with A# sensitivity, Einstein Telescope [11] and Cosmic Explorer [12,13], by scaling the result from the LIGO's O3 observing run. The cumulative memory SNR corresponding to triggers from a particular ground-based detector (d) with a run-time of T_{obs} [yr] is expressed as

$$\text{SNR}^d = \kappa \sqrt{T_{\text{obs}}} \sqrt{\int_{M_{\text{min}}}^{M_{\text{max}}} \int_{z_{\text{min}}}^{z_{\text{max}}^d(M)} \left[\frac{M^\alpha (1+z)^\alpha}{D_L(z)} \right]^2 \left[\sum_{\text{source}:s} \beta_s P_s(M) R_s(z) \right] \left[4\pi (D_C(z))^2 \frac{dD_C(z)}{dz} dz \right] dM}. \quad (24)$$

The double integral over redshift and mass essentially represents the expected sum of squared heights of the memory waveforms corresponding to all the triggers provided by detector d in one year of observation. From Eq. (17) we see that the SNR has a square-root dependence on this sum. For the purposes of this paper, we have chosen to restrict the calculation to equal mass binaries with the total mass ranging from $1M_\odot$ to 10^4M_\odot . The corresponding upper limit for the redshift integral is therefore given by the ground-based detector's redshift horizon $z_{\text{max}}^d(M)$, i.e., the maximum redshift at which an equal mass binary of total mass M can be detected with an SNR of 8. These redshift horizon curves are computed (and plotted in Fig. 9) for Advanced LIGO with O3 and A[#] sensitivities, Einstein Telescope, and Cosmic explorer using the GitHub code referenced in Ref. [22]. Thus, the domain of integration is represented by the area under the horizon redshift curves (albeit for computational purposes of circumventing singularities in the luminosity distance expression at $z = 0$, we employ a lower redshift cutoff of $z_{\text{min}} = 0.01$ which is the closest source that the LVK has measured to date).

The integrand (which is independent of the ground-based detector's sensitivity) is a product of the following terms: The first term, $\frac{M^\alpha (1+z)^\alpha}{D_L(z)}$, is essentially proportional to the height of the memory contribution of a single event with total mass M at a luminosity distance $D_L(z)$ [from Eq. (20)]. The second term, $\sum_{\text{source}:s} \beta_s P_s(M) R_s(z)$, is the rate density per unit comoving volume per unit time at which binaries of total mass M occur (units of $\frac{\text{Number}}{M_\odot \text{ Gpc}^3 \text{ yr}}$). β_s represents the relative abundance of a formation channel, $P_s(M)$ represents the normalized initial mass function (IMF) for that channel, and $R_s(z)$ represents the corresponding rate. In this paper, we have assumed globular clusters (GC) and isolated field binaries (IF) as the dominant formation channels with the relative abundance of $\beta_{\text{GC}} = \beta_{\text{IF}} = 0.5$ [23]. The IMF for field binaries, P_{IF} , is assumed to be a power law distribution [24] while the one for globular clusters, P_{GC} , is assumed to be log-uniform [25]. The corresponding rates as a function of redshift have been taken from Refs. [12,23]. The third term in the integrand, $4\pi (D_C(z))^2 \frac{dD_C(z)}{dz}$, represents the infinitesimal comoving volume element, with $D_C(z)$ representing the radial comoving distance. The cosmological model that gives the expressions for $D_L(z)$ and $D_C(z)$ is assumed to be the Λ CDM cosmology derived by the Planck Collaboration [26].

Having defined all the terms in Eq. (24), Table I shows the ratio of the rate of memory SNR accumulation in LISA by using projected LIGO A[#], ET and CE catalogs with the

SNR accumulation in LISA using the existing LIGO O3 catalog as a baseline. Additionally, an estimate for the runtime required for a $\text{SNR} = 5$ detection is also computed. The results suggest that memory detection with LISA, given a lifetime of 10 yr, is possible only if we use ET or ET in combination with CE. This comes from ET having the larger horizon redshift for high mass binaries compared to other ground-based detectors as shown in Fig. 9.

V. PROSPECTS OF MEMORY DETECTION WITH FUTURE LISA-LIKE MISSIONS

In addition to LISA we expect some more LISA-like mission concepts to be up and running after LISA's science operation in the second half of the century, some examples being ALIA, AMIGO, and Folkner. The corresponding results for these missions are presented in Table II. In this section, we take a look at each one of them briefly.

AMIGO's white paper document [9] entails a configuration identical to LISA (with 2.5 Gm arms and the same measurement band) but predicts a tenfold reduction in acceleration noise and an approximate tenfold reduction in shot noise achieved by using a 30 W laser in conjunction with a slightly bigger telescope diameter of 0.5 m. This in turn leads to an approximate tenfold improvement in the memory SNR and a 100-fold improvement in the time required to detect the memory effect.

ALIA's design [8] entails an equilateral triangle with 0.5 Gm arms leading to a slightly higher measurement band. Additionally, there is a projected 40000-fold increase in received power which leads to a 200-fold improvement of the shot noise limited displacement sensitivity which combined with the arm length reduction results in a 40-fold increase in the shot noise limited strain sensitivity, $\frac{40}{\sqrt{5}}$ -fold increase in the memory SNR and consequently a 320-fold improvement in the time required for memory detection.

In contrast to ALIA and AMIGO, Folkner's interferometer configuration [10] entails a 260 Gm equilateral triangle, thus targeting frequencies below the LISA band. In the shot noise limit, the increase in arm length is compensated by the reduced power received at the photodetector, thus leading to an almost identical strain sensitivity (a factor of $\sqrt{2/3}$ improvement coming from using a 3 W transmit laser instead of a LISA's 2 W laser). One challenge in using the shot-noise-dominated limit for Folkner is the fact that most of its frequency band is dominated by the galactic confusion noise, the resolution of which is unclear to date. That being said, assuming the galactic confusion noise is resolvable, we gain memory

SNR primarily due to the increased integration time over a round-trip (factor of $10.2\sqrt{3/2}$ in SNR and 156 in the time required for detection).

VI. CONCLUSION AND FUTURE PROSPECTS

In this article we propose a simple data analysis procedure to detect Christodoulou’s nonlinear gravitational memory effect using LISA’s (and future LISA-like mission’s) data stream and the event catalog of ground-based detectors. The idea is to first use the detection catalog of ground-based to get arrival times of detected events and then stack up with optimal weight factors, data snippets from the TDI data stream that start at these arrival times. This is followed up by computing the SNR in time domain by running the composite data stream through a matched filter with a triangular pulse being the template. Using simple astrophysical population models of binary black holes (Sec. IV) and the memory SNR derived from the existing LIGO O3 catalog, Table II provides estimates for the time required for the cumulative memory SNR in LISA and future space-based missions like AMIGO, ALIA and Folkner to cross the SNR threshold of 5 for catalogs derived from CE, ET, LIGO with A[#] and O3 sensitivities. Results suggest that LISA in conjunction with ET will most likely be able to detect the gravitational memory effect in a few years of concurrent operation and the results for the beyond LISA missions look even more promising.

While we do believe that the work done provides good baseline estimates and a time domain data analysis method to detect gravitational memory in space-based detectors, there are a few refinements that one can look into. Most of these involve relaxing assumptions to make the estimate more accurate.

- (1) Extending the calculation for unequal mass case. This would involve having to calculate and include higher-order spherical harmonic contributions [27] in Eq. (2) and having to modify Eq. (24) to an integral over both mass components.
- (2) As mentioned in Sec. I, in this work we assume perfect knowledge of the sign of the memory effect. In practice, for each trigger provided by the ground-based detector the sign of the memory effect has to be measured, for instance by using degeneracy breaking parameters constructed out of higher-order modes [4,5].
- (3) We could avoid the SNR loss due to the θ, ϕ orientation angles by splitting the sky in sections and assigning a template for each sky section instead of having a universal triangular pulse template.

Waveforms corresponding to oblique incidence angles resemble kinked triangular pulses with reduced heights (e.g., orange trace in Fig. 4). Thus in addition to using different templates for each sky section, we would also need to update the corresponding optimum weight factors used for stacking the data streams.

- (4) While in this work we look for memory signals in the TDI_{1,0} X data stream, eventually it will be useful to extend the calculations with TDI_{2,0} data streams accounting for varying arm lengths over one round-trip light travel time. Intuitively, we do not expect drastic changes from the estimates provided here.

ACKNOWLEDGMENTS

We thank Bernard Whiting for fruitful discussions. Additionally, this work is supported by National Aeronautics and Space Administration (NASA) Grants No. 80NSSC20K0126 and No. 80NSSC19K0324 for which we thank NASA for funding the research. Finally, this research uses the publicly available data from the LVK Collaboration’s observing runs and we acknowledge the following data statement: “This research has made use of data or software obtained from the Gravitational Wave Open Science Center, a service of LIGO Laboratory, the LIGO Scientific Collaboration, the Virgo Collaboration, and KAGRA. LIGO Laboratory and Advanced LIGO are funded by the United States National Science Foundation (NSF) as well as the Science and Technology Facilities Council (STFC) of the United Kingdom, the Max-Planck-Society (MPS), and the State of Niedersachsen/Germany for support of the construction of Advanced LIGO and construction and operation of the GEO600 detector. Additional support for Advanced LIGO was provided by the Australian Research Council. Virgo is funded, through the European Gravitational Observatory (EGO), by the French Centre National de Recherche Scientifique (CNRS), the Italian Istituto Nazionale di Fisica Nucleare (INFN) and the Dutch Nikhef, with contributions by institutions from Belgium, Germany, Greece, Hungary, Ireland, Japan, Monaco, Poland, Portugal, and Spain. The construction and operation of KAGRA are funded by Ministry of Education, Culture, Sports, Science and Technology (MEXT), and Japan Society for the Promotion of Science (JSPS), National Research Foundation (NRF) and Ministry of Science and ICT (MSIT) in Korea, Academia Sinica (AS) and the Ministry of Science and Technology (MoST) in Taiwan.”

- [1] D. Christodoulou, *Phys. Rev. Lett.* **67**, 1486 (1991).
- [2] A. G. Wiseman and C. M. Will, *Phys. Rev. D* **44**, R2945 (1991).
- [3] B. P. Abbott *et al.* (LIGO Scientific Collaboration and Virgo Collaboration), *Phys. Rev. Lett.* **116**, 061102 (2016).
- [4] P. D. Lasky, E. Thrane, Y. Levin, J. Blackman, and Y. Chen, *Phys. Rev. Lett.* **117**, 061102 (2016).
- [5] A. M. Grant and D. A. Nichols, *Phys. Rev. D* **107**, 064056 (2023).
- [6] S. Gasparotto, R. Vicente, D. Blas, A. C. Jenkins, and E. Barausse, [arXiv:2301.13228](https://arxiv.org/abs/2301.13228).
- [7] K. Danzmann *et al.*, [arXiv:1702.00786](https://arxiv.org/abs/1702.00786).
- [8] J. Crowder and N. J. Cornish, *Phys. Rev. D* **72**, 083005 (2005).
- [9] V. Baibhav *et al.*, *Exp. Astron.* **51**, 1385 (2021).
- [10] W. Folkner, A non-drag-free gravitational-wave mission architecture (2011), <https://pcos.gsfc.nasa.gov/studies/rfi/GWRFI-0003-Folkner.pdf>.
- [11] S. Kroker and R. Nawrodt, *IEEE Instrum. Measur. Mag.* **18**, 4 (2015).
- [12] M. Evans *et al.*, [arXiv:2109.09882](https://arxiv.org/abs/2109.09882).
- [13] D. Reitze *et al.*, *Bull. Am. Astron. Soc.* **51**, 035 (2019), <https://ui.adsabs.harvard.edu/abs/2019BAAS...51g..35R/abstract>.
- [14] A. K. Divakarla, Memory effects in the era of gravitational-wave astronomy, Ph.D. thesis, University of Florida, 2021.
- [15] S. L. Larson, W. A. Hiscock, and R. W. Hellings, *Phys. Rev. D* **62**, 062001 (2000).
- [16] M. Tinto, F. B. Estabrook, and J. W. Armstrong, *Phys. Rev. D* **65**, 082003 (2002).
- [17] M. Hewitson, E. Fitzsimons, and W. Weber, LISA performance model and error budget, Report No. LISA-AEI-INST-TN-003, 2020.
- [18] R. Abbott *et al.* (LIGO Scientific Collaboration and Virgo Collaboration), *Phys. Rev. X* **11**, 021053 (2021).
- [19] R. Abbott *et al.* (The LIGO Scientific Collaboration, The Virgo Collaboration, and The KAGRA Collaboration), Gwtc-3: Compact binary coalescences observed by LIGO and Virgo during the second part of the third observing run (2021), [arXiv:2111.03606](https://arxiv.org/abs/2111.03606).
- [20] D. Brown, Searching for gravitational radiation from binary black hole machos in the galactic halo, Ph.D. thesis, The University of Wisconsin–Milwaukee, 2004.
- [21] R. Abbott *et al.*, *SoftwareX* **13**, 100658 (2021).
- [22] H.-Y. Chen, D. E. Holz, J. Miller, M. Evans, S. Vitale, and J. Creighton, *Classical Quantum Gravity* **38**, 055010 (2021).
- [23] K. K. Y. Ng, S. Vitale, W. M. Farr, and C. L. Rodriguez, *Astrophys. J. Lett.* **913**, L5 (2021).
- [24] K. Belczynski, T. Ryu, R. Perna, E. Berti, T. L. Tanaka, and T. Bulik, *Mon. Not. R. Astron. Soc.* **471**, 4702 (2017).
- [25] C. L. Rodriguez and A. Loeb, *Astrophys. J.* **866**, L5 (2018).
- [26] J. Alves, F. Combes, A. Ferrara, T. Forveille, and S. Shore, *Astron. Astrophys.* **594**, E1 (2016).
- [27] C. Talbot, E. Thrane, P. D. Lasky, and F. Lin, *Phys. Rev. D* **98**, 064031 (2018).